Article

Transmission Enhancement through Sub-Wavelength Aperture Based on Regulable Water-Based Metamaterial

Pengfei Shi [1], Xiaodong Li [1], Hongge Zhao [1], Youfu Tang [1], Jingwei Zhu [1,*], Renjing Gao [2,*] and Shutian Liu [2]

1   College of Marine Electrical Engineering, Dalian Maritime University, Dalian 116026, China
2   State Key Laboratory of Structural Analysis for Industrial Equipment, Dalian University of Technology, Dalian 116023, China
*   Correspondence: zjwdl@dlmu.edu.cn (J.Z.); renjing@dlut.edu.cn (R.G.)

Abstract: A realization form of the Mie resonance with adjustable characteristics based on a water-based metamaterial is proposed. A novel local electromagnetic field coupling mechanism based on a water-based metamaterial is established, which is used for transmission enhancement through the sub-wavelength aperture for the first time. The water-based metamaterial particle for transmission enhancement at a specific frequency is designed. By designing the microfluidic control system to control the water filling (i.e., height) of the metamaterial particle, the adjustable transmission enhancement characteristics are realized. The influence of bilateral symmetry and flexible deformation of the metamaterial particle on the transmission characteristics is analyzed. The influence of the design parameters on the enhanced transmission characteristics is discussed.

Keywords: water-based metamaterial; enhanced transmission; reconfigurable metamaterial

1. Introduction

Electromagnetic metamaterial (EM MTM) is a kind of artificial medium composed of a periodic array or aperiodic sub-wavelength artificial units. It shows some unusual EM characteristics for different forms of incident waves, such as artificial plasma characteristics, negative reflection/refraction, EM stealth, Epsilon near zero, etc. [1–4]. It has shown a great application potential in communication, wireless power transmission, sensors, and other corresponding fields [5–8]. Following the deepening of the theoretical research and the innovation of the preparation process, a variety of EM MTM implementation forms were generated, including nano metamaterials, inverse-designed metastructures, multifunctional metamaterials, metallic patch MTM, and ceramic-based all-dielectric MTM [9–13]. However, there is still the need to further develop flexibility and controllability; that is, to realize unusual EM characteristics and reconfiguration in a broad band. Exploring a new realization form of the EM response and developing an easy-to-operate characteristic controlling method can provide diversified solutions for MTM to meet different background requirements.

Water-based EM MTM is a kind of all-dielectric MTM, which was made of deionized water. Because of its high permittivity, water-based particles with a reasonable shape or water-based arrays with a reasonable arrangement are easy to show the characteristics of all-dielectric MTM. Therefore, water-based MTM was proposed [14,15]. Based on Mie resonance, the water-based MTM has been designed to generate ultra-wideband absorption, toroidal moment, a beam-forming array, and so on [16–20]. The water-based MTM showed an excellent regulation performance. In one way, its EM response characteristics can be thermally adjusted by heating to change the dielectric permittivity of water [21]. However, it needs a long reaction time. In another way, the EM response characteristics can be adjusted by the water-based particle reshaping. Due to the excellent fluidity of water, the water-based MTM can be reshaped by filling and draining water in the container, mechanically rotating [22–24]. However, at present, there are few corresponding researches.

Research on the design and reconfiguration methods of water-based MTM was needed, and its application still needs to be further expanded. Finding the relationship between the appropriate configuration or size of the water-based MTM and its working frequency for a different physical background was required.

Enhanced transmission (ET) through sub-wavelength aperture is a special EM phenomenon in which the EM wave can pass through the aperture without being limited by the aperture's size. Ebbesen introduced a plasma structure near the sub-wavelength aperture to generate coupling between both sides of the metallic film, so as to break the limitation of the transmission efficiency and achieve ET [25]. Enlightened by this research, many different MTM forms were introduced into the ET design, containing the LC resonant metallic patched MTM and the Mie resonance-based ceramic all-dielectric MTM [26–28]. A reasonable water-based MTM will generate Mie scattering by itself to realize the spatial coupling near the aperture. Meanwhile, the water can be filled and drained in the container in real time through external mechanisms. Depending on the good shape following the characteristics of water, the flexible deformation of the container can increase the regulation of the EM characteristics. The reaction time was short. The water-based MTM was an ideal realization form for the controllable ET.

Based on the above analysis, a method for controlling the Mie resonance characteristics by adjusting the water level of water-based MTM was proposed. A real-time controllable sub-wavelength aperture ET implementation method based on water-based MTM was established. The feasibility and the flexible controllability of the water-based MTM in ET were verified by a simulation and experiment.

2. Design of Water-Based MTM for ET

The transmission system discussed was enclosed in a rectangular waveguide. The incident wave can propagate through the waveguide. It would be blocked by a metallic film, even if there was a sub-wavelength aperture in the film. The water-based MTM was considered to be applied to enhance the wave propagation. At room temperature, the dielectric permittivity of the water satisfied the first-order Debye formula within the frequency range discussed, which was described as [17]:

$$\varepsilon(\omega, T_{water}) = \varepsilon_\infty(T_{water}) + \frac{\varepsilon_0(T_{water}) - \varepsilon_\infty(T_{water})}{1 - i\omega\tau(T_{water})} \tag{1}$$

where $\varepsilon_\infty(T_{water})$ and $\varepsilon_0(T_{water})$ are the optical permittivity and static permittivity, respectively. τ is the rotational relaxation time. When the particle size was much lower than the working wavelength, the particle can be regarded as circular scattering particles. Under the lowest order resonance, the MTM particle will show the characteristics of electric dipole or magnetic dipole. The normalized electric polarizability or magnetic polarizability was expressed as:

$$\alpha_e = p/\varepsilon_0 a^3 E, \; \alpha_m = m/\mu_0 a^3 H \tag{2}$$

where p and m are the electric and magnetic dipole moments of the single particle excited by the electric field and magnetic field. Under the external field excitation, with a proper structure, the MTM particle can generate Mie resonance. If it was placed near the sub-wavelength aperture and the electric/magnetic dipoles were formed in the particle that radiated energy through the sub-wavelength aperture. The space on both sides of the film was coupled and ET in the transmission system was achieved. Formula (2) also indicated that the characteristics of the magnetic dipole/electric dipole were determined by the configuration of the particle. It was an easy way to control the coupling characteristics by adjusting the shape of water-based particles through water filling and drainage.

When the microstructure was electrically small (the dimension was much smaller than the working wavelength), its EM response can be described by some equivalent analyzing model, such as the circuit model [29–31]. The equivalent circuit model was introduced to analyze the mechanism of the resonance of the water-based MTM particle [30,31]. At the

surface of the particle, the normal component of the displacement current was continuous and expressed as:

$$- \mathrm{i}\omega(\varepsilon - \varepsilon_0)\vec{E}_0 \cdot \vec{\mathrm{n}} = \mathrm{i}\omega\varepsilon_0\vec{E}_{\mathrm{dip}} \cdot \vec{\mathrm{n}} + \mathrm{i}\omega\varepsilon\vec{E}_{\mathrm{res}} \cdot \vec{\mathrm{n}} \tag{3}$$

where $\vec{\mathrm{n}}$ is outward unit vector normal to the particle surface. $\vec{E}_{\mathrm{res}}$ is the difference between the electric field inside the particle $\vec{E}_{\mathrm{int}}$ and the incident part $\vec{E}_{\mathrm{insi}}$. In Equation (3), the integration of each part over the surface would represent the displacement current in a different branch, i.e.,

$$I_{\mathrm{dis}} = I_{\mathrm{sph}} + I_{\mathrm{fringe}} \tag{4}$$

where I_{dis} is the total displacement current. I_{sph} is the displacement current from the inside of the particle and I_{fringe} is the displacement current from the fringe field. The relationship of the displacement current above can also be regarded as the current in the branches at a node in the circuit, which satisfied the Kirchhoff's law. The MTM particle was regarded as immersed in the surrounding environment. The electric field would be different according to the boundary conditions, the shape of the particle, and the material properties, while in the excitation of the incident wave, the field response inside and outside all the dielectric particles can still be equivalent to a basic parallel circuit with basic circuit elements, as shown in Figure 1a. At the specific frequency, the inside part was regarded as an impedance Z_1 branch which consisted of a resistor R_1 and capacitor C paralleled circuit. The outside part was an impedance Z_2 branch which consisted of a resistor R_2 and inductor L series circuit. The equivalent capacitance or inductance characteristics of the dielectric was dependent on the sign of the real part of the material permittivity ε. The non-zero imaginary part of ε would generate an equivalent resistor. The impedance in each branch can be expressed as:

$$Z_1 = R_1 // (j\omega L) \tag{5}$$

$$Z_2 = R_2 + 1/j\omega C \tag{6}$$

(a)

(b)
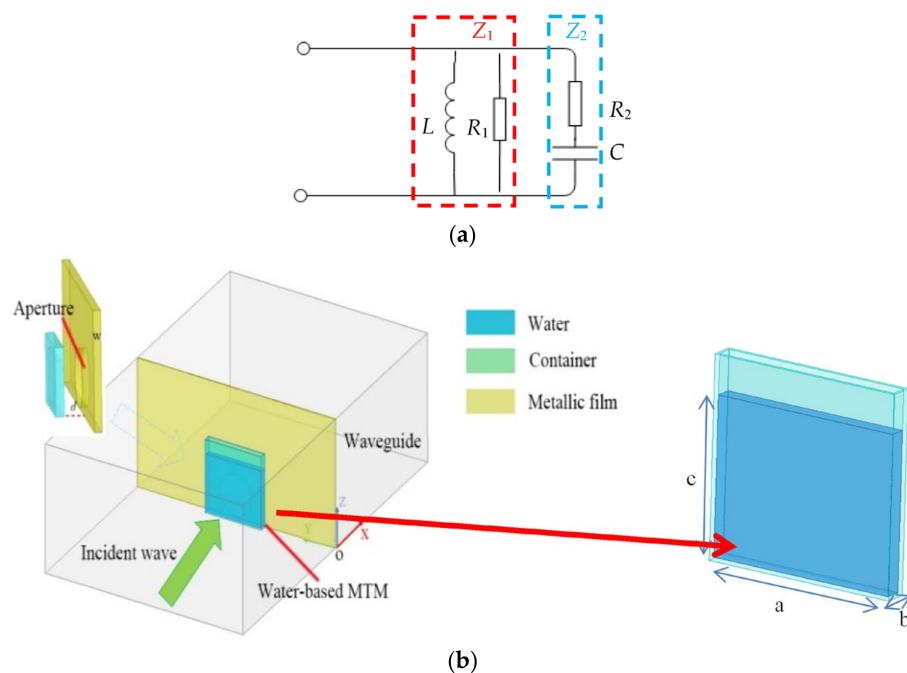
Figure 1. (**a**) The equivalent circuit model of the water-based particle. (**b**) Schematic diagram of the waveguide system and the water-based MTM particle.

The total impedance of the circuit was $Z_1//Z_2$. The variation in the external environment would cause the difference in Z_2. When the reactance was zero at a certain frequency, the system can generate resonance to make a local field enhancement.

The working frequency of interest from 0.76 GHz to 1.15 GHz was selected. The corresponding standard rectangular waveguide was 200 mm × 247.65 mm × 123.82 mm. Two rectangular waveguides were connected and sandwiched a w = 0.5 mm thick metallic film. A subwavelength aperture was drilled on the film. The origin was set at the vertex of the bottom edge of the film. The coordinate of the center of the aperture was (0, 123.825 mm, 21 mm) and its radius r was 20 mm, which was far less than the wavelength of the incident wave ($r = \lambda/15$). The cuboid water-based particle was in front of the film. The Debye model, Formula (1), indicated that the permittivity of the water would decrease as the working frequency increases. Since the frequency band discussed was low and in a narrow band, it was considered that the permittivity of the water remained at 80. The tangent loss was 0.025. To obtain the ET characteristics, 1 GHz was desired. The distance between the water-based MTM and the metallic film d can be adjusted. It would affect the coupling strength between the spaces on both sides of the film. In order to facilitate the adjustment of the shape of the particle, it was considered that the particle and the film were not close to each other. In this example, d was set as 0.8 mm. Through parametric sweeping and optimization, the size of the MTM particle was determined as $a \times b \times c$ = 69.6 mm × 5.8 mm × h, where h represented the water level. A container was used to hold and shape the water. Its material was polylactic acid (PLA), whose permittivity was 2.5. The thickness of its wall was 0.8 mm. The ET system is shown in Figure 1b. This structure was taken as a feasible base structure and was gradually reconfigured to analyze its adjusted characteristics.
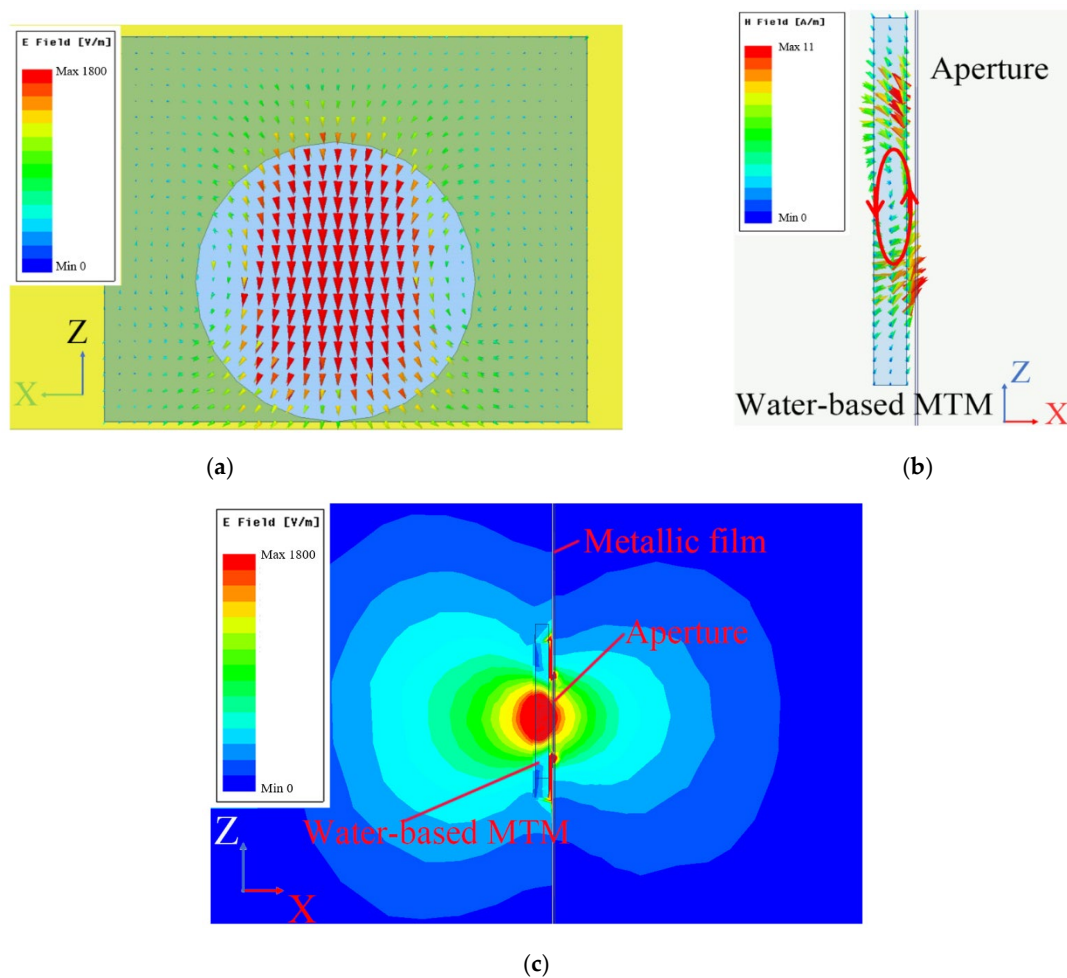
The transmission characteristics of the system were calculated by numerical simulation software Ansys HFSS. The wave port was added on both sides of the air box as the input and output. The other four surfaces of the air box were covered by the perfect conductor to simulate the metallic waveguide. Without water-based MTM, S_{21} in the full frequency band was below −30 dB, as the green dashed–dotted line shown in Figure 2. When the designed water-based MTM with 52 mm h was placed at the preset region, the system exhibited −9.97 dB S_{21} at 1 GHz, as the blue solid line shows in Figure 2. A strong coupling and the ET characteristics at the desired frequency were achieved.
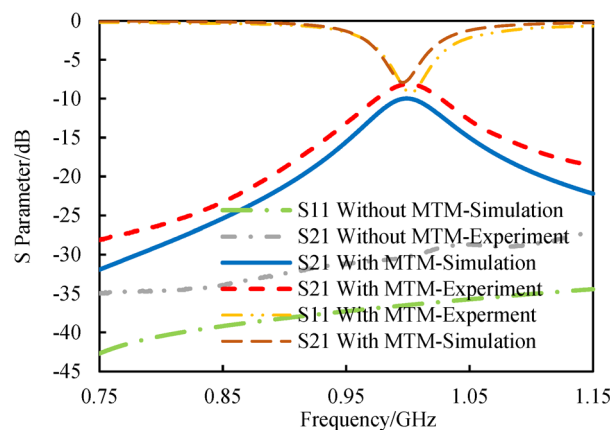
Figure 2. The simulated and experimental S parameters of the waveguide system with or without the water-based MTM.

The local electric field and magnetic field vector in the MTM particle at 1 GHz was plotted in Figure 3a,b. The magnetic field formed a single annular distribution in the X-Z plane, which was equivalent to an electric dipole. The resonance of the effective permittivity and permeability was generated by the MTM particle. The MTM resonance produced a strong field distribution near the aperture which coupled the space on both

sides (Figure 3c). The wave was localized in the water-based particle. The MTM particle, as a radiation source, emitted the wave into the secondary space of the waveguide to make the wave propagate to the output. In contrast, without MTM, the wave was cut off at the aperture.

(a)

(b)

(c)

Figure 3. (**a**) The electric field and (**b**) the magnetic field vector in the water. (**c**) The electric field distribution in the waveguide.

The transmission characteristics of the waveguide system were tested. The experimental platform was composed of the vector network analyzer (VNA), two standard rectangular waveguides, and the microfluidic system, as shown in Figure 4a. the VNA was connected to the input and output ports of the waveguide through the coaxial cable and the waveguide coaxial converter. The perforated metallic film was clamped between the two rectangular waveguides. The water-based MTM prototype was placed near the aperture. The microfluidic system can regulate the water content of the particle. PLA was chosen as the raw material, and 3D printing technology was introduced to fabricate the container. Water was injected into the container through the soft capillary. The waveguide and the prototype were shown in Figure 4b.
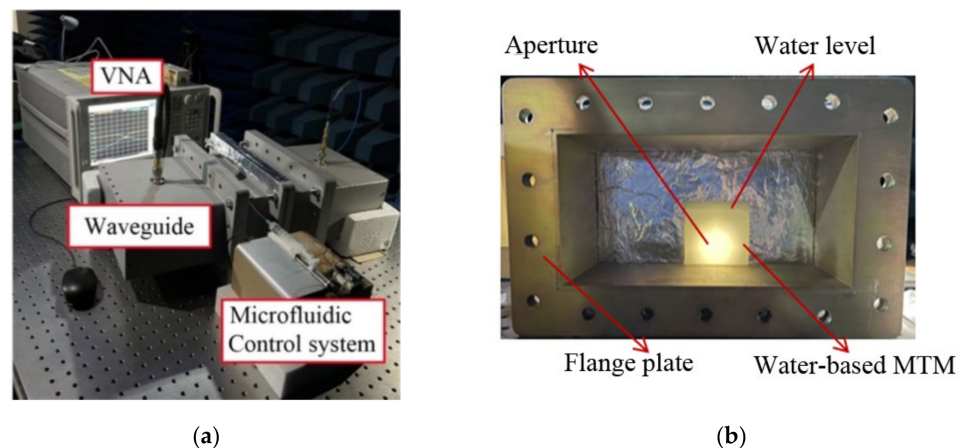
Figure 4. (**a**) The experimental platform and (**b**) the prototype.

At room temperature, without water-based MTM, the measured S_{21} of the waveguide system was below -30 dB in the whole frequency band, as the dotted grey line shows in Figure 2. When the designed water-based MTM was placed at the preset region, there was an obvious passing band. The peak of S_{21} was -9.12 dB at 1 GHz, as the red dashed line shows in Figure 2. The water-based MTM significantly enhanced the transmission of the system. The measured peak frequency was the same as the desired one. The feasibility of the designed water-based particle was proved. The maximum transmission efficiency obtained in the experiment was slightly different with that in the simulation. That was mainly because the differences between the material loss of the water were set in the simulation and in the experiment. In addition, the container manufacturing error also had an impact on the experimental results.

3. The MTM Configuration Adjustment and Reconfiguration

3.1. The Water Level Adjustment

The shape of the water-based particle can be adjusted by controlling the water filling volume in the container (the height of the particle h) in this design. As h gradually rose from 45 mm to 70 mm with a step of 5 mm, the simulated resonant frequency of the system decreased from 1.03 GHz to 0.97 GHz, and the transmission efficiency almost remained unchanged (Figure 5a). When h was 45 mm, the transmission peak owned a maximum value of -9.56 dB at 1.03 GHz. When h exceeded 70 mm, the resonant frequency and the maximum transmission efficiency basically remained constant.

The water filling volume (i.e., height) of the water-based particle was adjusted by the microfluidic system, which was mainly composed of an AT89C series microcontroller, stepper motor, and microflow syringe. When the microcontroller program started to control the progress of the small-sized stepping motor, the micro syringe was pushed forward to control the continuous rise of the height h. The S_{21} parameters of the transmission system with the water-based MTM were measured. As h increased from 45 mm to 70 mm, the peak frequency gradually shifted from 1.05 GHz to 0.95 GHz (Figure 5b). The resonant frequency can be effectively controlled by the designed microfluidic system. The tested transmission efficiency of ET was in a good agreement with the simulated one.
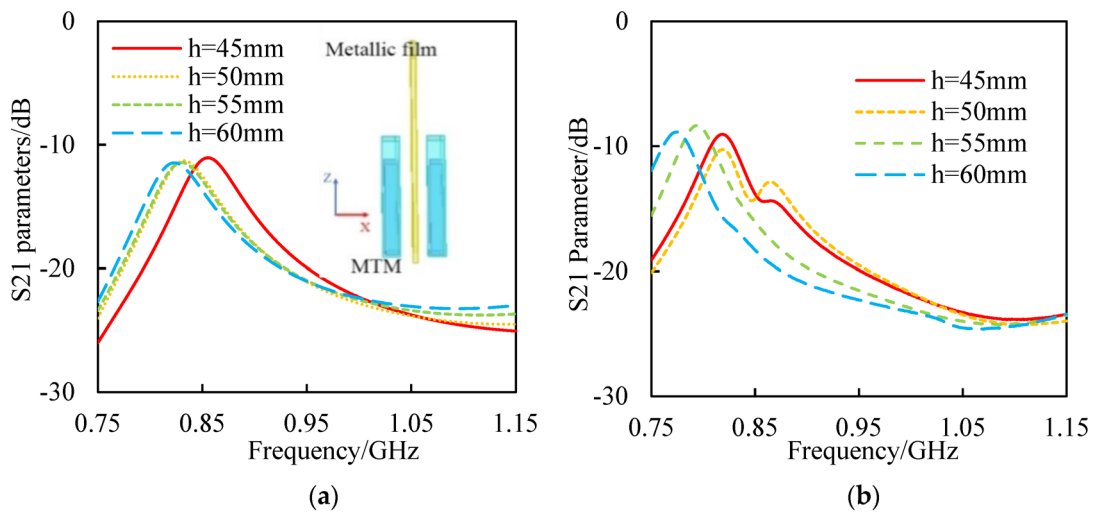
3.2. The Symmetry of the Water-Based MTM Particle

The ET characteristics of the bilaterally symmetric water-based MTM, which consisted of two water-based particles placed on both sides of the aperture, were analyzed. With a reasonable particle structure, the bilaterally symmetric MTM can effectively induce double resonance coupling on either side of the aperture which helps to improve the ET transmission efficiency. For comparative analysis, the same particle size and position as the unilateral structure was adopted. The peak frequency would exceed the range of the waveguide cut-off frequency when h was greater than 60 mm, so h was only considered

to be adjusted from 45 mm to 60 mm. The simulated highest S_{21} of the system with the bilaterally symmetric water-based MTM would be near -10 dB (Figure 6a), and the tested highest S_{21} of the system was -8.3 dB (Figure 6b). As h increased, S_{21} shifted gradually from 0.867 GHz to 0.830 GHz from the simulation and shifted from 0.818 GHz to 0.774 GHz from testing. Due to the reflection impedance between the primary and secondary particles, the S_{21} peak generated by the bilaterally symmetric water-based MTM was red-shifted compared with that of the unilateral water-based MTM.
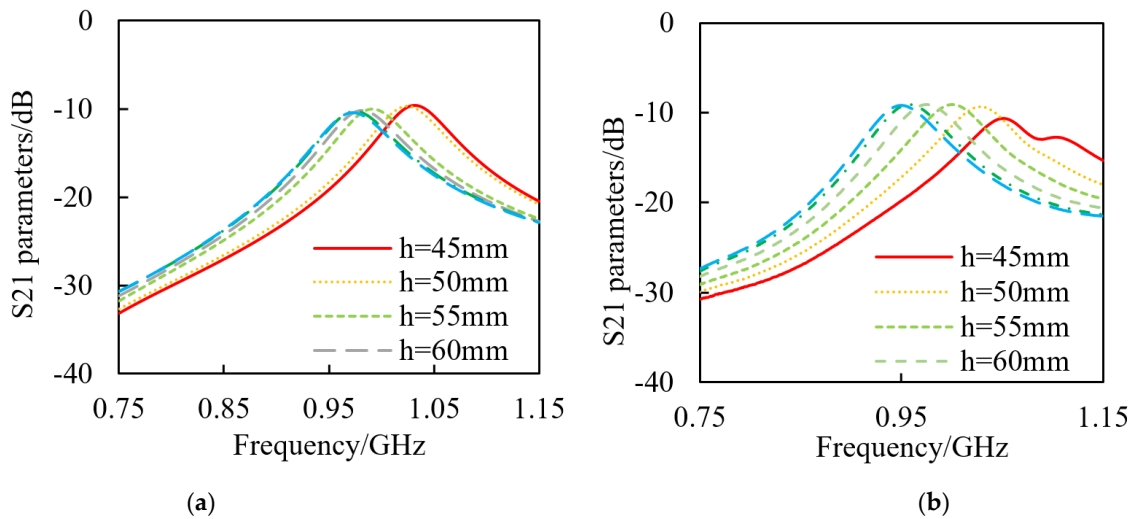
Figure 5. S_{21} parameters of the system with the unilateral water-based MTM particle with different water height from (**a**) simulation and (**b**) experiment.


Figure 6. S_{21} parameters with the bilaterally symmetric MTM particle with different water height from (**a**) simulation, (**b**) experiment.

3.3. Flexible Deformation of Water-Based MTM Particle

The influence from the flexible deformation on the transmission system was analyzed. Appropriate external stress extrusion or stretching will cause the elastic deformation of MTM, which will increase the adjustable parameters and make it more controllable. The ET characteristics of the water-based MTM particles with a different curvature radius were simulated. The material for the container's fabrication can be changed to rubber so that the MTM particles can be bended and expanded. Compared with PLA, rubber has a soft texture and a good mechanical operability. Under a normal temperature, water has a good

shape following property, so the shape of the water-based particle can be consistent with the rubber container. Following the deformation of the rubber container, the water-based particle can be easily bent and partially deformed.

The length of the water-based MTM particle *a* was kept constant. The container was bent along the *Z* axis with a different curvature radius (R = 30 mm, 45 mm). $R = \infty$ meant that the particle was kept flat. Because it was inconvenient to deform the planar MTM by applying external stress in the waveguide, the curved MTM container was 3D printed with PLA directly. PLA was still selected as the material of the container in the simulation and experiment. The simulated S_{21} of the particles were shown in Figure 7a. The water-based particle with a certain flexible deformation can still realize ET. As the radius of the curvature gradually decreased, the peak frequency shifted from 1 GHz to 1.08 GHz gradually. The high transmission efficiency at the peak frequency was still maintained. The transmission characteristics of the bent MTM particle with a curvature radius of 30 mm were tested. As shown in Figure 7b, the curved MTM particle showed a -9.78 dB peak of S_{21} at 1.095 GHz, which was similar to the simulated one. The phase did not show a sudden change.
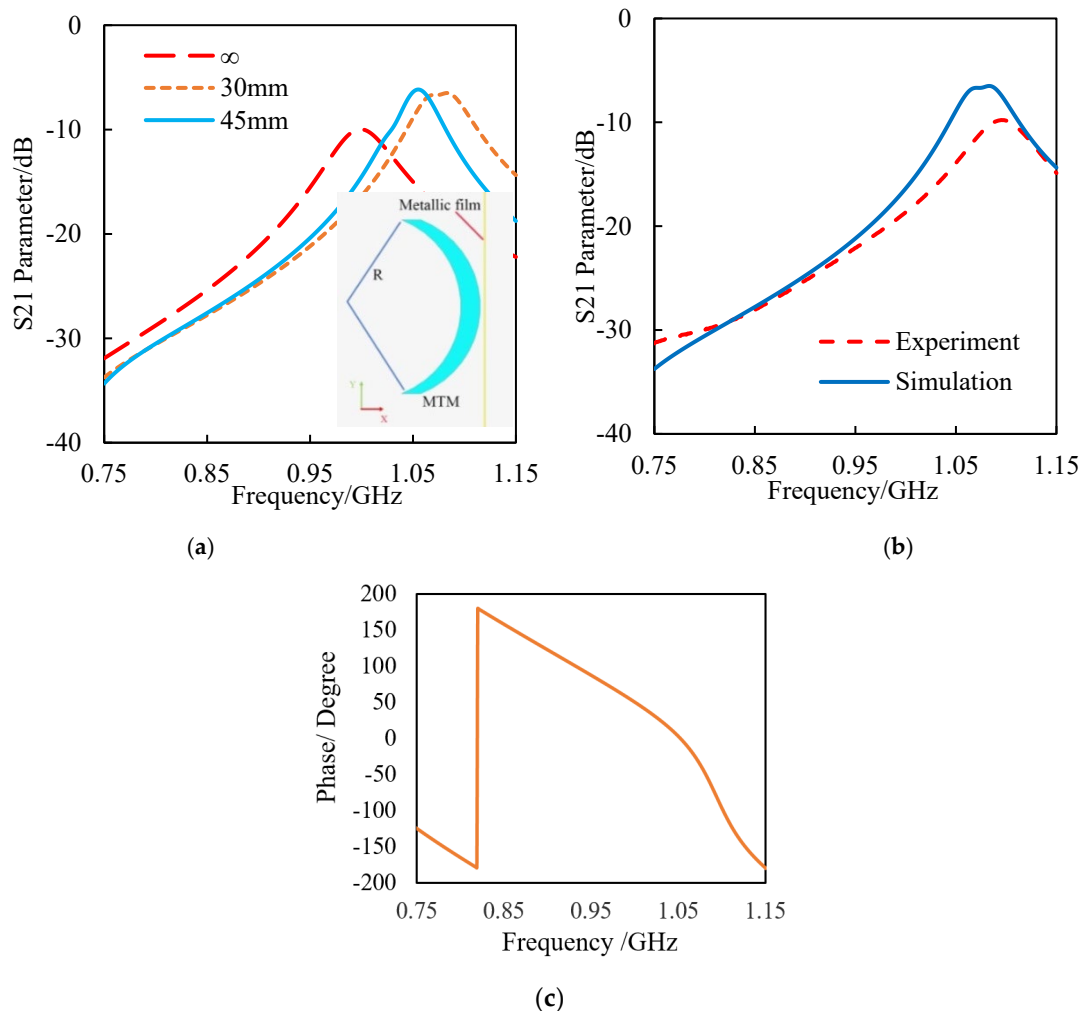
Figure 7. (**a**) The simulated S_{21} parameters with curved MTM with different curvature radius. (**b**) The simulated and tested magnitude of S_{21} parameters and (**c**) the simulated phase of S_{21} parameters when the curvature radius of the MTM particle was 30 mm.

4. Discussion

The above water-based MTM design was based on the consideration of the resolution of the water level adjustment and the controllability of the bending deformation. Setting the thickness *a* to a small value made the MTM easy to bend and to reshape. However,

the proposed design parameters for ET were not unique. On the premise of ensuring Mie resonance at the required specific frequency, the initial design parameters of the MTM particle can be redesigned. The influence on the transmission characteristics from the size of the MTM particle and the distance between the MTM particle and the film was discussed. The limitation of the design, the future improvement, and the potential application were also discussed at last.

### 4.1. The Influence of the Distance between the Particle and the Film

The influence of the distance between the MTM particle and the film was analyzed. The size of the MTM particle remained unchanged, and the distance was adjusted from 0 mm to 10 mm. It was found, while the distance changed from 0 mm to 10 mm, that the distance mainly made the center working frequency of the ET shift, as shown in Figure 8. When the distance was small, the amplitude change caused by the change in the distance was limited. At this time, the output part of the waveguide acted as a secondary resonant circuit. The reflection impedance generated by the secondary resonant circuit acted on the primary circuit and affected its resonant frequency. At this distance, the coupling coefficient between the two circuits was not significantly affected. When the distance was greater than 7 mm, the ET amplitude at the working frequency decreased significantly (-11.8 dB at 1.06 GHz). The excessive distance seriously weakened the coupling strength between the two coupling parts.
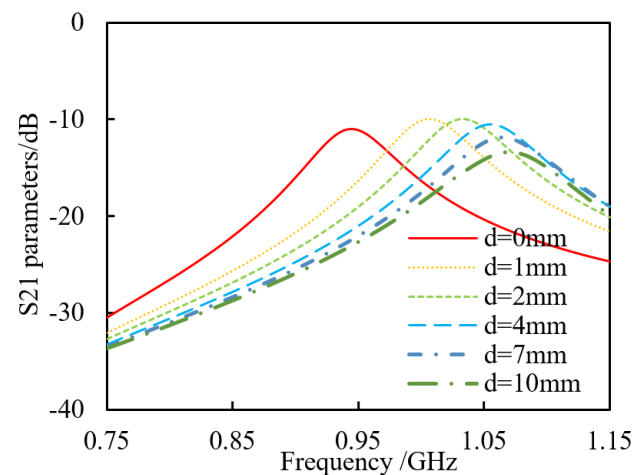
Figure 8. The simulated S_{21} parameters with different distances from film.

4.2. The Influence of the Size Parameters of the Particle

Using the particles with a small thickness *b* was conducive to the controllability of the bending deformation. Under this requirement, the area of the designed particle covered the whole aperture. However, if the particle did not cover the aperture, whether the transmission characteristics would be improved should also be analyzed. In order to achieve ET at a specific working frequency, the relationship between the water-based particle size and the distance from the particle to the film *d* was not unique. There were still a few feasible solutions. One more feasible solution of the MTM design parameters was found at the required working frequency. The corresponding size optimized by the MTM particle is shown in Figure 9a. The required ET working frequency was also at 1 GHz. The designed particle was $a \times b \times c = 42$ mm $\times$ 12.8 mm $\times$ 37.8 mm. The distance *d* = 0 mm. The particle designed in Section 2, fully covering the aperture, was taken as a comparison. As shown in Figure 9b, both the MTM particles can achieve ET at 1 GHz. The two particles only showed a slight difference in the ET characteristics. Compared with the fully covered aperture by the MTM, the partial exposure of the aperture would not improve the transmission efficiency significantly.
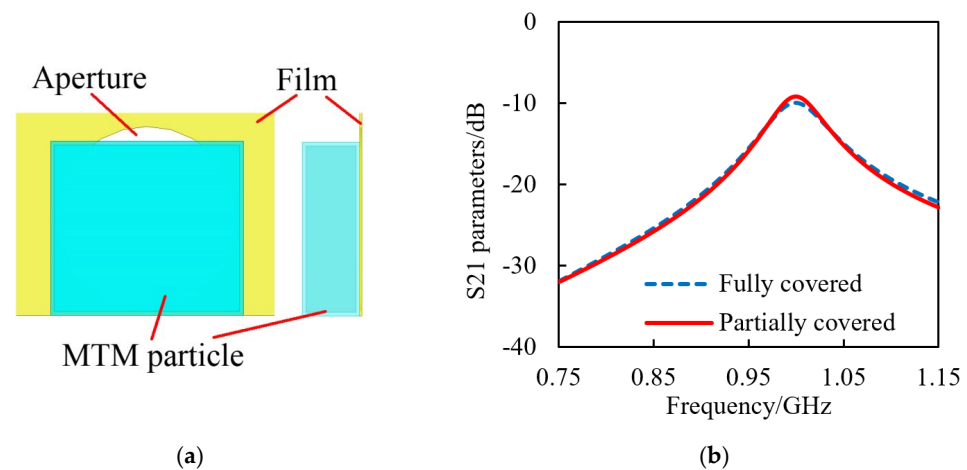
Figure 9. (**a**) The MTM particle partially covering the aperture and (**b**) the simulated S_{21} parameters of the system with the MTM particle partially covering the aperture.

4.3. Future Improvement for the Limitations and the Potential Application

In the water-based MTM ET system, the loss in the water was a little high, which was mainly due to the material characteristics of the water. In this water-based MTM design, the loss of the water was about 0.3. In further research, if the liquidity of the particle was kept and the loss was reduced, the ET efficiency can be improved while maintaining the controllability through appropriate methods.

The water-based MTM particle with a specific shape and size can produce transmission at the required frequency in the designed ET system. This property not only can produce certain frequency selection characteristics in communication and wave absorption systems, but it also exhibited a potential application in the field of sensing. Because the water level, shape, and dielectric constant of water-based MTM particles had a corresponding relationship with the resonant frequency, the monitoring of the state or structural characteristics of the water-based particle fillers can be realized by tracking the peak frequency and amplitude of the S parameters.

5. Conclusions

In this paper, a method to realize water-based MTM with tunable properties based on Mie scattering was proposed. The dielectric container was designed to shape the water, and the microfluidic system was introduced to adjust the water filling. The MTM realized the enhanced transmission through the sub-wavelength aperture at the required frequency. The correlation between the ET working frequency and the water level in the MTM particle was established. The adjustment methods of the transmission characteristics, including symmetry and elastic deformation, were developed. A small distance between the MTM particle and the film mainly affected the peak frequency of the system, while an excessive distance would reduce the coupling strength on both sides of the film.

References

1. Huidobro, P.A.; Silveirinha, M.G.; Galiffi, E.; Pendry, J.B. Homogenization theory of space-time metamaterials. *Phys. Rev. Appl.* **2021**, *16*, 14044. [CrossRef]
2. Huang, Q.; Wang, G.; Zhou, M.; Zheng, J.; Tang, S.; Ji, G. Metamaterial electromagnetic wave absorbers and devices: Design and 3D microarchitecture. *Sci. Technol.* **2022**, *108*, 90–101. [CrossRef]
3. Ye, K.P.; Pei, W.J.; Sa, Z.H.; Chen, H.; Wu, R.X. Invisible gateway by superscattering effect of metamaterials. *Phys. Rev. Lett.* **2021**, *126*, 227403. [CrossRef] [PubMed]
4. Pacheco-Pena, V.; Beruete, M.; Rodriguez-Ulibarri, P.; Engheta, N. On the performance of an ENZ-based sensor using transmission line theory and effective medium approach. *New J. Phys.* **2019**, *21*, 43056. [CrossRef]
5. Xin, L.; Qiufan, C.; Shiliang, G.; Zhiquan, L. Research of gate-tunable phase modulation metasurfaces based on epsilon-near-zero property of Indium-Tin-Oxide. *Photonics* **2022**, *9*, 323.
6. Sun, K.; Fan, R.; Zhang, X.; Zhang, Z.; Shi, Z.; Wang, N.; Xie, P.; Wang, Z.; Fan, G.; Liu, H.; et al. An overview of metamaterials and their achievements in wireless power transfer. *J. Mater. Chem. C* **2018**, *6*, 2925–2943. [CrossRef]
7. Hu, J.; Bandyopadhyay, S.; Liu, Y.H.; Shao, L.Y. A review on metasurface: From principle to smart metadevices. *Front. Phys.* **2021**, *8*, 586087. [CrossRef]
8. Lalegani, Z.; Ebrahimi SA, S.; Hamawandi, B.; Spada, L.L.; Batili, H.; Toprak, M.S. Targeted dielectric coating of silver nanoparticles with silica to manipulate optical properties for metasurface applications. *Mater. Chem. Phys.* **2022**, *287*, 126250. [CrossRef]
9. Estakhri, N.; Edwards, B.; Engheta, N. Inverse-designed metastructures that solve equations. *Science* **2019**, *363*, 1333–1338. [CrossRef]
10. Greybush, N.J.; Pacheco-Pena, V.; Engheta, N.; Murray, C.B.; Kagan, C.R. Plasmonic Optical and Chiroptical Response of Self-Assembled Au Nanorod Equilateral Trimers. *ACS Nano* **2019**, *13*, 1617–1624. [CrossRef]
11. Lincoln, R.L.; Scarpa, F.; Ting, V.P.; Trask, R.S. Multifunctional composites: A metamaterial perspective. *Multifunct. Mater.* **2019**, *2*, 043001. [CrossRef]
12. Pengfei, S.; Yu, Q.; Yangyang, C.; Hongge, Z.; Renjing, G.; Shutian, L. Topology optimization of metamaterial microstructure for wireless power transfer with high power transmission efficiency. *J. Magn. Magn. Mater.* **2021**, *537*, 168228.
13. Nemkov, N.A.; Stenishchev, I.V.; Basharin, A.A. Nontrivial nonradiating all-dielectric anapole. *Sci. Rep.* **2017**, *7*, 1064. [CrossRef]
14. Rybin, M.V.; Filonov, D.S.; Samusev, K.B.; Belov, P.A. Phase diagram for the transition from photonic crystals to dielectric metamaterials. *Nat. Commun.* **2015**, *6*, 10102. [CrossRef]
15. Liu, L.; Katko, A.R.; Li, D.; Cummer, S.A. Broadband electromagnetic metamaterials with reconfigurable fluid channels. *Phys. Rev. B* **2014**, *89*, 245132. [CrossRef]
16. Odit, M.; Kapitanova, P.; Andryieuski, A.; Belov, P.; Lavrinenko, A.V. Experimental demonstration of water based tunable metasurface. *Appl. Phys. Lett.* **2016**, *109*, 11901. [CrossRef]
17. Andryieuski, A.; Kuznetsova, S.M.; Zhukovsky, S.V.; Kivshar, Y.S.; Lavrinenko, A.V. Water: Promising opportunities for tunable all-dielectric electromagnetic metamaterials. *Sci. Rep.* **2015**, *5*, 13535. [CrossRef]
18. Jacobsen, R.E.; Lavrinenko, A.; Arslanagic, S. Water-Based Metasurfaces for Effective Switching of Microwaves. *IEEE Antennas Wireless Propag.Lett.* **2018**, *17*, 571–574. [CrossRef]
19. Ren, J.; Yin, J.Y. Cylindrical-water-resonator-based ultra-broadband microwave absorber. *Opt. Mater Express* **2018**, *8*, 2060–2071. [CrossRef]
20. Xie, J.; Zhu, W.; Rukhlenko, I.D.; Xiao, F.; He, C.; Geng, J.; Liang, X.; Jin, R.; Malin, P. Water metamaterial for ultra-broadband and wide-angle absorption. *Opt. Express* **2018**, *26*, 5052–5059. [CrossRef]
21. Zhou, Y.; Shen, Z.; Wu, J. Design of ultra-wideband and near-unity absorption water-based metamaterial absorber. *Appl. Phys. B* **2020**, *126*, 52. [CrossRef]
22. Stenishchev, I.V.; Basharin, A.A. Toroidal response in all-dielectric metamaterials based on water. *Sci. Rep.* **2017**, *7*, 9468. [CrossRef] [PubMed]
23. Jacobsen, R.E.; Lavrinenko, A.V.; Arslanagić, S. A water-based huygens dielectric resonator antenna. *IEEE Open J. Antennas Propag.* **2020**, *1*, 493–499. [CrossRef]
24. Xu, J.; Fu, Q.; Fan, Y.; Nan, J.; Zhang, F. Thermally Reconfigurable Fano Resonance in Water Brick Pair Metamaterial. *Results Phys.* **2021**, *28*, 104650. [CrossRef]
25. Ebbesen, T.W.; Lezec, H.J.; Ghaemi, H.F.; Thio, T.; Wolff, P.A. Extraordinary optical transmission through sub-wavelength hole arrays. *Nature* **1998**, *391*, 667–669. [CrossRef]
26. Guo, Y.; Liu, S.; Bi, K.; Lei, M.; Zhou, J. Low-power nonlinear enhanced electromagnetic transmission of a subwavelength metallic aperture. *Photon. Res.* **2018**, *6*, 1102–1106. [CrossRef]
27. Ramaccia, D.; Palma, L.D.; Ates, D.; Ozbay, E.; Toscano, A.; Bilotti, F. Analytical model of connected bi-Omega: Robust particle for the selective power transmission through sub-wavelength apertures. *IEEE Trans. Antennas Propag.* **2014**, *62*, 2093–2101. [CrossRef]
28. Takou, E.; Tasolamprou, A.C.; Tsilipakos, O.; Viskadourakis, Z. Anapole tolerance to dissipation losses in thermally tunable water-based metasurfaces. *Phys. Rev. Appl.* **2021**, *15*, 14043. [CrossRef]
29. Vegni, L.; Cicchetti, R.; Capece, P. Spectral dyadic Green's function formulation for planar integrated structures, IEEE Trans. *Antennas Propag.* **1988**, *36*, 1057–1065. [CrossRef]

30. Donnelly, E.; Spada, L.L. Electromagnetic and thermal nanostructures: From waves to circuits. *Eng. Res. Express* **2020**, *2*, 15045. [CrossRef]
31. Engheta, N.; Salandrino, A.; Alu, A. Circuit Elements at Optical Frequencies: Nanoinductors, Nanocapacitors, and Nanoresistors. *Phys. Rev. Lett.* **2005**, *95*, 95504. [CrossRef]